CLASSIFICATION OF EXOPLANETS ACCORDING TO DENSITY

Andrzej Odrzywolek[a,b,†], Johann Rafelski[a]

[a]Department of Physics, The University of Arizona, Tucson, AZ 85721, USA
[b]M. Smoluchowski Institute of Physics, Jagiellonian University, Kraków, Poland

(Received July 5, 2018; accepted August 28, 2018)

Considering probability distribution as a function of the average density $\bar{\rho}$ computed for 424 extrasolar planets, we identify three log-normal Gaussian population components. The two most populous components at $\bar{\rho} \simeq 0.7$ g/cc and $\bar{\rho} \simeq 7$ g/cc are the ice/gas giants and iron/rock super-Earths, respectively. A third component at $\bar{\rho} \simeq 30$ g/cc is consistent with brown dwarfs, *i.e.*, electron degeneracy supported objects. We note presence of several extreme density planetary objects.

1. The raw radius–mass data

Our objective is to recognize statistical regularities and possible anomalies in the physical state of the matter according to density [1] addressing the databases of exoplanets [2–4]. The average density $\bar{\rho}$ of the planets

$$\bar{\rho} = \frac{M}{\frac{4}{3}\pi R^3} \tag{1}$$

is closely related to the theoretical mass–radius (M–R) relation [5].

A source of the data is the NASA exoplanet archive, `exoplanetarchive.ipac.caltech.edu` [6] and The Extrasolar Planets Encyclopedia, `exoplanet.eu` [7]. Both were retrieved on October 22, 2016. Number of objects reported with both M and R is 510 out of 3388 and 610 out of 3533, respectively. To ensure quality of data, we concatenated databases, merged duplicates and split into "gold", "silver" and "bronze" subsets. The "gold" sample of 424 includes only exoplanets data with consistent (but not necessarily identical) and unambiguous values M, R in both sources, and reviewed in original sources [8–10] all dubious cases. "Silver", including 146 objects, includes unconfirmed results appearing only once, and the remaining "bronze" data includes ~ 100 upper mass limits only.

† Corresponding author: `andrzej.odrzywolek@uj.edu.pl`

In this analysis, only the "gold" sample plus eight Solar System planets were used. The here considered raw M–R data is presented visually in Fig. 1. Curved line shows the theoretical radius–mass relation for a pure Fe planet [11]. Solar System planets are marked by +. The resulting histogram for base-10 logarithm of the density is shown in Fig. 2, using 32-bins chosen for visual convenience.

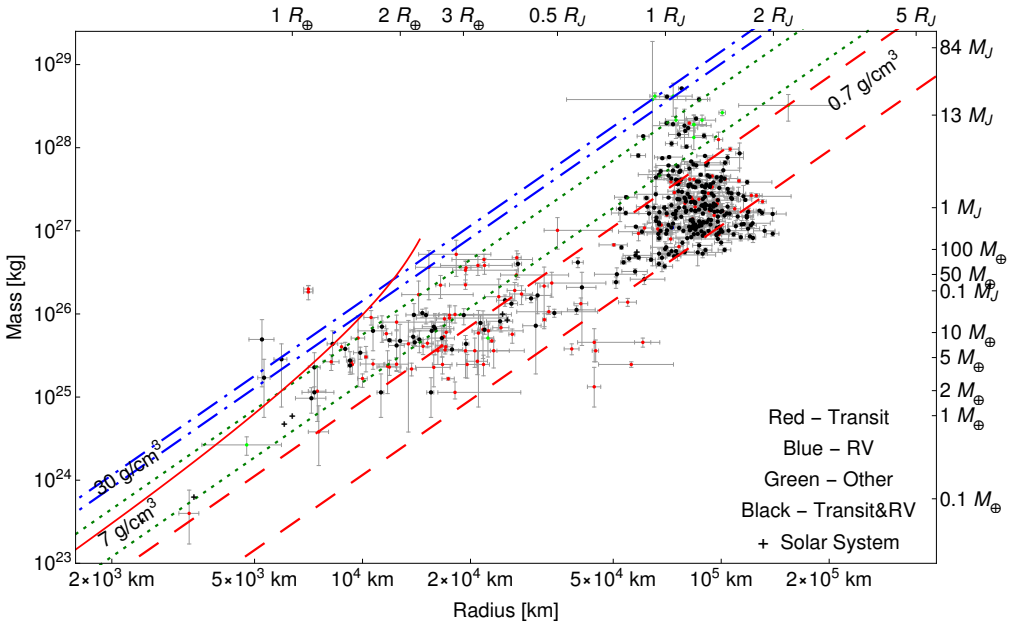

Fig. 1. (Color online) Scatter plot in mass–radius plane (log scale) of raw data for 432 (exo)planets. Data points are color coded (online only) according to detection method: red: transit; blue: radial velocity (RV); green: imaging, microlensing; black: both RV and transit. Diagonal lines along constant average density delimit 1σ-domains identified in our analysis as belonging to the three main families of exoplanets, see the text.

Three low-density outliers below 0.05 g/cc (leftmost/yellow bars in Fig. 2: Kepler-51 b,c,d [12]) and three high-density above 50 g/cc (rightmost/orange bars in Fig. 2: Kepler-128 b,c [8], Kepler-131 c [10]) are also visible in Fig. 1 below and respectively, above the diagonal lines. These are separated from the bulk of data and are excluded from the statistical analysis.

2. Data analysis

Wolfram Mathematica 11 `EstimatedDistribution` command [13] was used to process our data set of 418 exoplanets (424 less 6 outliers) + 8 So-

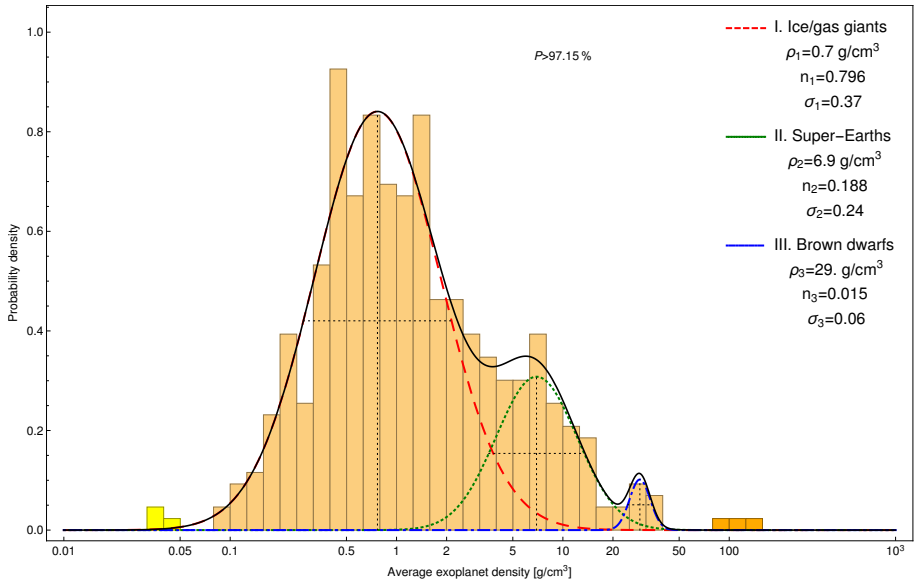

Fig. 2. (Color online) Distribution of the average density for 424 exoplanets and 8 Solar System planets. Histogram of 32 data bins is shown for visualization purpose only; our fit uses the density data directly. Interpretation/names of the component curves is based on the study of average density only.

lar System planets. Log-likelihood maximum for the data is the continuous black curve shown in Fig. 2. This result suggests that the probability density for exoplanet data $\bar{\rho}$ is the superposition of three log-normal Gaussian distributions.

The two biggest Gaussian components in Fig. 2 (dashed/red and dotted/green lines) can be recognized in the density distribution figure before the numerical fit. A third smaller component (dot-dashed/blue line) emerges as an additional component during numerical treatment. Values for positions $\bar{\rho}_k$, normalizations n_k, and standard deviations σ_k of the three Gaussians are shown within contents of Fig. 2. The Pearson χ^2 probability test shows a value above $P > 97.15\%$ for the 3-Gaussian probability density function shown in Fig. 2.

The envelope curve seen in Fig. 2 for exoplanet data is thus a superposition of three dimensionless probability distributions

$$\frac{\mathrm{d}P}{\mathrm{d}\lg\bar{\rho}} = \rho\frac{\mathrm{d}P}{\mathrm{d}\bar{\rho}}\,. \tag{2}$$

A probability distribution normal in $\lg\bar{\rho}$ could be due to extraneous factors such as data sampling during observation, but it could also be related to scale-free planet formation mechanisms.

3. Proposed classification of exoplanets

We classify the populations from left to right in Fig. 2; the names of the components are based in our intuitive expectation and prior knowledge. Since distributions overlap objects within a given density range, they may not be of the same nature.

I. **Ice/gas.** The first and dominant ($P_I \simeq 80\%$) population depicted as a dashed/red line and centered at $\rho_I = 0.7$ g/cc in Fig. 2 corresponds to the Saturn/Uranus/Jupiter planet type. Considering the full width at half maximum (FWHM), the distribution extends from $\rho \simeq 0.3$ g/cc to $\rho \simeq 2.1$ g/cc (Fig. 2, dotted horizontal segment). Members of this population are found predominantly between dashed/red diagonal lines in Fig. 1.

II. **Iron/rock.** The second component ($P_e \simeq 19\%$, $\rho_e = 6.9$ g/cc, FWHM from 3.6 to 13.4 g/cc, with objects found between dotted/green diagonal lines in Fig. 1) is shown as a dotted/green line in Fig. 2. These objects are very near to Earth's average density of 5.5 g/cc. This is so-called super-Earth population, *i.e.*, planets with composition similar to Earth, but often more massive, see *e.g.* [15], Fig. 6.

III. **Degenerate.** The third and smallest component ($P_d \simeq 1.5\%$, $\rho_d \simeq 30$ g/cc, at FWHM extending from 25 to 34 g/cc, *cf.* Fig. 1, dot-dashed/blue bands) is shown as a dot-dashed/blue line in Fig. 2. This density domain overlaps with electron degenerate matter, *i.e.* brown dwarfs [14, 16].

Since the three population classes are *overlapping* in density, the individual object planet class membership is to be understood in a statistical sense. For example, according to the proposed classification, the Earth, given the average density 5.5 g/cc, has 4.4 times less chance to be an ice giant than super-Earth object. It is possible that with more abundant and precise exoplanet data and allowing for additional information (*e.g.* range of M and R; surface composition), the classification can be made more precise. The super-Earths normalization ($P_e = 19\%$) is smaller than expected based on Solar System experience ($P_e \simeq 50\%$). This could be a result of a bias induced by observational methods available today that favor detection of M and R for large objects as we note visually in Fig. 1.

4. Conclusions

Understanding of mean density distribution for exoplanets offers a convenient tool to identify the new and mysterious in the Universe. The knowledge of the widths of the population distributions allows to realize presence

of anomalies when larger exoplanet data base becomes available. Our analysis results thus lay out the basis for the discovery of new classes of rare objects, *e.g.* CUDO [18], dark matter [17] or strange matter [19] contaminated exoplanets. Indeed, three small ultra-dense outliers are a tantalizing indication of mysteries that the future exoplanet results may reveal.

We proposed that the extrasolar planet distribution is a superposition of three log-normal Gaussians population components allowing the introduction of three classes of exoplanetary objects, distinguishing these by average density. The two classes (I ice/gas giants, 80% and II super-Earths, 19%) dominate the available data. Our classification in terms of density agrees with the Solar System situation where outer and inner planets are in classes I and II, respectively. The observed relative normalization of the components, strongly favoring the ice/gas class, is probably an observational bias. This bias is also the reason why we do not divide the results seen in Fig. 1 into domains according to M–R ranges as the eye easily captures.

The degenerate class III includes about 1.5% of the available objects among 432. In mathematical analysis, a separate population can be assigned. On the other hand, 2×3 outliers removed from the fit are too few to be assigned their own population class. These outliers are inconsistent with the derived probability distribution function (PDF) at 94% confidence level in the sense of conservative Pearson χ^2 test, this inconsistency is higher (97.1%) if low/high density are considered separately. When more data becomes available, it will be possible to decide if the two groups of three density outlier exoplanets are a data fluctuation or, more interestingly, a new population.

The proposed classification method employing average density statistics can be used to analyze growing data sets on other astrophysical objects: stars including white dwarfs, neutron stars, and minor bodies of the Solar System, analysis of which is currently underway.

A.O. work was supported by The Kosciuszko Foundation. A.O. thanks the Department of Physics, University of Arizona for kind hospitality.

REFERENCES

[1] V.F. Weisskopf, *Science* **187**, 605 (1975).
[2] J. Hecht, *Nature* **530**, 272 (2016).
[3] A. Witze, *Nature* **527**, 288 (2015).
[4] J.J. Lissauer, R.I. Dawson, S. Tremaine, *Nature* **513**, 336 (2014).
[5] A.W. Howard, *Science* **340**, 572 (2013).
[6] R.L. Akeson *et al.*, *Publ. Astron. Soc. Pacific* **125**, 989 (2013).

[7] J. Schneider *et al.*, *Astron. Astrophys.* **532**, A79 (2011).
[8] J.-W. Xie, *Astrophys. J. Suppl. Ser.* **210**, 25 (2014).
[9] S. Hadden, Y. Lithwick, *Astrophys. J.* **787**, 80 (2014).
[10] G.W. Marcy *et al.*, *Astrophys. J. Suppl. Ser.* **210**, 20 (2014).
[11] L. Zeng, D. Sasselov, *Publ. Astron. Soc. Pacific* **125**, 227 (2013).
[12] K. Masuda, *Astrophys. J.* **783**, 53 (2014).
[13] Wolfram Research Inc., 'Wolfram — Alpha Knowledgebase", 2016.
[14] A. Burrows, W.B. Hubbard, J.I. Lunine, J. Liebert, *Rev. Mod. Phys.* **73**, 719 (2001).
[15] E.A. Petigura *et al.*, *Astrophys. J.* **811**, 102 (2015).
[16] A. Burrows, J. Liebert, *Rev. Mod. Phys.* **65**, 301 (1993).
[17] J. Diemand, B. Moore, J. Stadel, *Nature* **433**, 389 (2005).
[18] J. Rafelski, L. Labun, J. Birrell, *Phys. Rev. Lett.* **110**, 111102 (2013).
[19] G.L. Shaw, M. Shin, M. Desai, R.H. Dalitz, *Nature* **337**, 436 (1989).